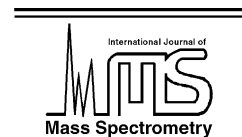




ELSEVIER

International Journal of Mass Spectrometry 220 (2002) 445–448



www.elsevier.com/locate/ijms

## Subject index Volume 220

### Ab initio calculation

- A G2(+) level investigation of the gas-phase identity nucleophilic substitution at neutral oxygen, 1
- Catalysis models for the enolization of the acetaldehyde radical cation, 53

### Absolute photoionisation cross-sections

- A time-of-flight mass spectrometry study of the fragmentation of valence shell ionised benzene, 31

### Acetone

- Reactions of size-selected protonated water clusters  $H^+(H_2O)_n$  ( $n = 2-6$ ) with an acetone molecule in a guided ion beam apparatus, 375

### Actinide

- Gas-phase reactions of bare and oxo-ligated actinide and lanthanide cations with pentamethylcyclopentadiene studied in a quadrupole ion trap mass spectrometer, 419

### Anion clusters

- Infrared spectra of the  $F^-CH_4$  and  $Br^-CH_4$  anion complexes, 273

### Arginine

- Molecular recognition of arginine in small peptides by supra-molecular complexation with dibenzo-30-crown-10 ether, 87

### Bath gas effect

- Gas-phase reactions of bare and oxo-ligated actinide and lanthanide cations with pentamethylcyclopentadiene studied in a quadrupole ion trap mass spectrometer, 419

### Benzene

- Fission mechanisms of doubly charged organic molecular clusters, 99

### Calcium isotope analysis

- Measurement of calcium isotopes ( $\delta^{44}Ca$ ) using a multicollector TIMS technique, 385

### Caloric curve

- Caloric curve for the liquid-to-gas transition of the  $H_{25}^+$  hydrogen cluster ion, 263

### $C_2F_5I$

- Electron attachment to  $C_2F_5I$  molecules and clusters, 211

### $C_2H_4$

- Photoionisation of ethylene clusters by synchrotron radiation in the energy range 17–50 eV, 281

### Charge separation reactions

- A time-of-flight mass spectrometry study of the fragmentation of valence shell ionised benzene, 31

### Charged complexes

- Infrared spectra of the  $F^-CH_4$  and  $Br^-CH_4$  anion complexes, 273

### CID

- Probing several structures of  $Fe(H_2O)_n^+$  and  $Co(H_2O)_n^+$  ( $n = 1, \dots, 10$ ) cluster ions, 111

### Cluster anion

- High resolution study of cluster anion formation in low-energy electron collisions with molecular clusters of  $CO_2$ ,  $CS_2$ , and  $O_3$ , 313

### Cluster fragmentation

- Caloric curve for the liquid-to-gas transition of the  $H_{25}^+$  hydrogen cluster ion, 263

### Cluster ions

- Probing several structures of  $Fe(H_2O)_n^+$  and  $Co(H_2O)_n^+$  ( $n = 1, \dots, 10$ ) cluster ions, 111
- Complete chemical conversion of  $[(NO)_m(CH_3OH)_n]^+$  to  $NO^+(CH_3ONO)_x$  ( $x=1-12$ ): experiment and theory, 145
- Unimolecular dissociation of non-stoichiometric oxygen cluster ions  $O_n^{+*}$  ( $n = 5, 7, 9, 11$ ): a switch from  $O_3$  to  $O_2$  loss above cluster size  $n = 5$ , 221

### Cluster size dependence

- Cage effects and rotational hindrance in the surface scattering of large  $(N_2)_n$  clusters, 159

### Clusters

- Fission mechanisms of doubly charged organic molecular clusters, 99
- Rydberg Matter of K and  $N_2$ : angular dependence of the time-of-flight for neutral and ionized clusters formed in Coulomb explosions, 127
- Modelling ionic nucleation in small neon clusters, 193
- Electron attachment to  $C_2F_5I$  molecules and clusters, 211
- Infrared spectroscopy of jet-cooled, electronically excited clusters of Coumarin 151: excited-state interactions and conformational relaxation, 231
- Photoionisation of ethylene clusters by synchrotron radiation in the energy range 17–50 eV, 281

### Cluster–surface interaction

- Cage effects and rotational hindrance in the surface scattering of large  $(N_2)_n$  clusters, 159

### Coincidence spectroscopy

- Fission mechanisms of doubly charged organic molecular clusters, 99
- Photoelectron–photofragment coincidence spectroscopy of  $NO_2^-(NO)_{1,2}$ : solvation effects of NO on  $NO_2^-$ , 253

- Collision cross section  
Expanded theory for the resolving power of a linear ion mobility spectrometer, 399
- Conformational  
Infrared spectroscopy of jet-cooled, electronically excited clusters of Coumarin 151: excited-state interactions and conformational relaxation, 231
- Coulomb explosions  
Rydberg Matter of K and N<sub>2</sub>: angular dependence of the time-of-flight for neutral and ionized clusters formed in Coulomb explosions, 127
- Crown ether  
Molecular recognition of arginine in small peptides by supramolecular complexation with dibenzo-30-crown-10 ether, 87
- Dimer radical cation  
Catalysis models for the enolization of the acetaldehyde radical cation, 53
- Disproportionation  
Photochemistry of (NO)<sub>n</sub><sup>-</sup> as studied by photofragment mass spectrometry, 137
- Dissociation  
Reactions of size-selected protonated water clusters H<sup>+</sup>(H<sub>2</sub>O)<sub>n</sub> (*n* = 2–6) with an acetone molecule in a guided ion beam apparatus, 375
- Dissociative electron attachment  
Electron attachment to C<sub>2</sub>F<sub>5</sub>I molecules and clusters, 211
- Double spike correction  
Measurement of calcium isotopes ( $\delta^{44}\text{Ca}$ ) using a multicollector TIMS technique, 385
- Doubly charged ions  
A photoionisation mass spectrometry study of the fragmentation of silicon tetrafluoride, tetrachloride and tetrabromide, 359
- Electron attachment  
Electron attachment to C<sub>2</sub>F<sub>5</sub>I molecules and clusters, 211  
High resolution study of cluster anion formation in low-energy electron collisions with molecular clusters of CO<sub>2</sub>, CS<sub>2</sub>, and O<sub>2</sub>, 313
- Electron impact  
Strong fragmentation of large rare gas clusters by high energy electron impact, 183
- Electrons  
The origin of electrons in MALDI and their use for sympathetic cooling of negative ions in FTICR, 11
- Energy exchanges  
Cage effects and rotational hindrance in the surface scattering of large (N<sub>2</sub>)<sub>n</sub> clusters, 159
- Enolization  
Catalysis models for the enolization of the acetaldehyde radical cation, 53
- Expectation values (Drift time)  
Expanded theory for the resolving power of a linear ion mobility spectrometer, 399
- Field ionisation  
Ionisation and fragmentation dynamics of laser desorbed polycyclic aromatic hydrocarbons using femtosecond and nanosecond post-ionisation, 69
- Fission  
Fission mechanisms of doubly charged organic molecular clusters, 99
- Formic acid  
Reactions of hydrated aluminum ions with methanol and formic acid, 331
- Fragmentation  
Strong fragmentation of large rare gas clusters by high energy electron impact, 183
- Fragmentation rates  
A time-of-flight mass spectrometry study of the fragmentation of valence shell ionised benzene, 31
- FTICR MS  
The origin of electrons in MALDI and their use for sympathetic cooling of negative ions in FTICR, 11
- Gas phase  
Molecular recognition of arginine in small peptides by supramolecular complexation with dibenzo-30-crown-10 ether, 87
- Gas-phase metal ion–molecule chemistry  
Gas-phase reactions of bare and oxo-ligated actinide and lanthanide cations with pentamethylcyclopentadiene studied in a quadrupole ion trap mass spectrometer, 419
- Halide–methane complexes  
Infrared spectra of the F<sup>-</sup>–CH<sub>4</sub> and Br<sup>-</sup>–CH<sub>4</sub> anion complexes, 273
- Heats of formation  
A photoionisation mass spectrometry study of the fragmentation of silicon tetrafluoride, tetrachloride and tetrabromide, 359
- Hydrated aluminum ion  
Reactions of hydrated aluminum ions with methanol and formic acid, 331
- Hydrogen bond  
Vibrational spectroscopic evidence of unconventional hydrogen bonds, 289
- Hydrogen cluster ions  
Caloric curve for the liquid-to-gas transition of the H<sub>25</sub><sup>+</sup> hydrogen cluster ion, 263
- Hydrogen formation  
Reactions of hydrated aluminum ions with methanol and formic acid, 331
- Incorporation  
Reactions of size-selected protonated water clusters H<sup>+</sup>(H<sub>2</sub>O)<sub>n</sub> (*n* = 2–6) with an acetone molecule in a guided ion beam apparatus, 375
- Induced current  
Expanded theory for the resolving power of a linear ion mobility spectrometer, 399
- Infrared  
Vibrational spectroscopic evidence of unconventional hydrogen bonds, 289

- Infrared spectra  
 Infrared spectra of the  $F^-CH_4$  and  $Br^-CH_4$  anion complexes, 273
- Infrared spectroscopy  
 Infrared spectroscopy of jet-cooled, electronically excited clusters of Coumarin 151: excited-state interactions and conformational relaxation, 231
- Ion cooling  
 The origin of electrons in MALDI and their use for sympathetic cooling of negative ions in FTICR, 11
- Ion mobility spectrometry (IMS)  
 Expanded theory for the resolving power of a linear ion mobility spectrometer, 399
- Ionization  
 Complete chemical conversion of  $[(NO)_m(CH_3OH)_n]^+$  to  $NO^+(CH_3ONO)_x$  ( $x=1-12$ ): experiment and theory, 145
- Jet-cooled  
 Infrared spectroscopy of jet-cooled, electronically excited clusters of Coumarin 151: excited-state interactions and conformational relaxation, 231
- Kinetic energy release  
 Unimolecular dissociation of non-stoichiometric oxygen cluster ions  $O_n^{+*}$  ( $n = 5, 7, 9, 11$ ): a switch from  $O_3$  to  $O_2$  loss above cluster size  $n = 5, 221$   
 A photoionisation mass spectrometry study of the fragmentation of silicon tetrafluoride, tetrachloride and tetrabromide, 359
- Lanthanide  
 Gas-phase reactions of bare and oxo-ligated actinide and lanthanide cations with pentamethylcyclopentadiene studied in a quadrupole ion trap mass spectrometer, 419
- Laser desorption/femtosecond laser mass spectrometry  
 Ionisation and fragmentation dynamics of laser desorbed polycyclic aromatic hydrocarbons using femtosecond and nanosecond post-ionisation, 69
- Magnetic Moment  
 $NH_3$  adsorption around  $Ni_n$  ( $n \leq 4$ ) clusters, 171
- MALDI  
 The origin of electrons in MALDI and their use for sympathetic cooling of negative ions in FTICR, 11
- Mass spectrum  
 Complete chemical conversion of  $[(NO)_m(CH_3OH)_n]^+$  to  $NO^+(CH_3ONO)_x$  ( $x=1-12$ ): experiment and theory, 145
- Matrix effects  
 High precision measurement of titanium isotope ratios by plasma source mass spectrometry, 21
- Metastable decay  
 Unimolecular dissociation of non-stoichiometric oxygen cluster ions  $O_n^{+*}$  ( $n = 5, 7, 9, 11$ ): a switch from  $O_3$  to  $O_2$  loss above cluster size  $n = 5, 221$
- Methanol  
 Fission mechanisms of doubly charged organic molecular clusters, 99
- Complete chemical conversion of  $[(NO)_m(CH_3OH)_n]^+$  to  $NO^+(CH_3ONO)_x$  ( $x=1-12$ ): experiment and theory, 145  
 Reactions of hydrated aluminum ions with methanol and formic acid, 331
- Methyl nitrite  
 Complete chemical conversion of  $[(NO)_m(CH_3OH)_n]^+$  to  $NO^+(CH_3ONO)_x$  ( $x=1-12$ ): experiment and theory, 145
- Modelling  
 Modelling ionic nucleation in small neon clusters, 193
- Molecular dynamics simulations  
 Cage effects and rotational hindrance in the surface scattering of large  $(N_2)_n$  clusters, 159
- Molecular recognition  
 Molecular recognition of arginine in small peptides by supramolecular complexation with dibenzo-30-crown-10 ether, 87
- Moment analysis (Peak width)  
 Expanded theory for the resolving power of a linear ion mobility spectrometer, 399
- Multicollector  
 Measurement of calcium isotopes ( $\delta^{44}Ca$ ) using a multicollector TIMS technique, 385
- Multiphoton  
 Complete chemical conversion of  $[(NO)_m(CH_3OH)_n]^+$  to  $NO^+(CH_3ONO)_x$  ( $x=1-12$ ): experiment and theory, 145
- Multiply charged ions  
 Ionisation and fragmentation dynamics of laser desorbed polycyclic aromatic hydrocarbons using femtosecond and nanosecond post-ionisation, 69
- Negatively charged clusters  
 Infrared spectra of the  $F^-CH_4$  and  $Br^-CH_4$  anion complexes, 273
- $NH_3$  adsorption  
 $NH_3$  adsorption around  $Ni_n$  ( $n \leq 4$ ) clusters, 171
- $Ni_n$  clusters  
 $NH_3$  adsorption around  $Ni_n$  ( $n \leq 4$ ) clusters, 171
- $NiNH_3$  clusters  
 $NH_3$  adsorption around  $Ni_n$  ( $n \leq 4$ ) clusters, 171
- Nitric oxide  
 Complete chemical conversion of  $[(NO)_m(CH_3OH)_n]^+$  to  $NO^+(CH_3ONO)_x$  ( $x=1-12$ ): experiment and theory, 145
- Nitric oxide cluster anion  
 Photochemistry of  $(NO)_n^-$  as studied by photofragment mass spectrometry, 137
- Nitrogen clusters  
 Cage effects and rotational hindrance in the surface scattering of large  $(N_2)_n$  clusters, 159
- Nitrogen oxides  
 Photoelectron-photofragment coincidence spectroscopy of  $NO_2^-(NO)_{1,2}$ : solvation effects of  $NO$  on  $NO_2^-$ , 253
- Nucleation  
 Modelling ionic nucleation in small neon clusters, 193
- Oxygen  
 Unimolecular dissociation of non-stoichiometric oxygen cluster ions  $O_n^{+*}$  ( $n = 5, 7, 9, 11$ ): a switch from  $O_3$  to  $O_2$  loss above cluster size  $n = 5, 221$

- Phase transition  
Caloric curve for the liquid-to-gas transition of the  $\text{H}_{25}^+$  hydrogen cluster ion, 263
- Photodetection  
Photoelectron–photofragment coincidence spectroscopy of  $\text{NO}_2^-(\text{NO})_{1,2}$ : solvation effects of NO on  $\text{NO}_2^-$ , 253
- Photofragmentation  
Probing several structures of  $\text{Fe}(\text{H}_2\text{O})_n^+$  and  $\text{Co}(\text{H}_2\text{O})_n^+$  ( $n = 1, \dots, 10$ ) cluster ions, 111  
Photochemistry of  $(\text{NO})_n^-$  as studied by photofragment mass spectrometry, 137
- Photoionisation  
Photoionisation of ethylene clusters by synchrotron radiation in the energy range 17–50 eV, 281
- Plasma source mass spectrometry  
High precision measurement of titanium isotope ratios by plasma source mass spectrometry, 21
- Polycyclic aromatic hydrocarbons (PAHs)  
Ionisation and fragmentation dynamics of laser desorbed polycyclic aromatic hydrocarbons using femtosecond and nanosecond post-ionisation, 69
- Potential energy surface  
Catalysis models for the enolization of the acetaldehyde radical cation, 53
- Proton affinity  
Reactions of size-selected protonated water clusters  $\text{H}^+(\text{H}_2\text{O})_n$  ( $n = 2-6$ ) with an acetone molecule in a guided ion beam apparatus, 375
- Protonated water clusters  
Reactions of size-selected protonated water clusters  $\text{H}^+(\text{H}_2\text{O})_n$  ( $n = 2-6$ ) with an acetone molecule in a guided ion beam apparatus, 375
- Proton-transfer catalysis  
Catalysis models for the enolization of the acetaldehyde radical cation, 53
- Quadrupole ion trap  
Gas-phase reactions of bare and oxo-ligated actinide and lanthanide cations with pentamethylcyclopentadiene studied in a quadrupole ion trap mass spectrometer, 419
- Rare gas cluster  
Strong fragmentation of large rare gas clusters by high energy electron impact, 183
- Reaction mechanism  
A G2(+) level investigation of the gas-phase identity nucleophilic substitution at neutral oxygen, 1
- Redox reactions  
Reactions of hydrated aluminum ions with methanol and formic acid, 331
- Rotational hindrance  
Cage effects and rotational hindrance in the surface scattering of large  $(\text{N}_2)_n$  clusters, 159
- Rydberg Matter  
Rydberg Matter of K and  $\text{N}_2$ : angular dependence of the time-of-flight for neutral and ionized clusters formed in Coulomb explosions, 127
- Rydberg states  
Rydberg Matter of K and  $\text{N}_2$ : angular dependence of the time-of-flight for neutral and ionized clusters formed in Coulomb explosions, 127
- $\text{S}_{\text{N}}2$  at neutral oxygen  
A G2(+) level investigation of the gas-phase identity nucleophilic substitution at neutral oxygen, 1
- Solvation  
Photoelectron–photofragment coincidence spectroscopy of  $\text{NO}_2^-(\text{NO})_{1,2}$ : solvation effects of NO on  $\text{NO}_2^-$ , 253
- Sputtering  
Strong fragmentation of large rare gas clusters by high energy electron impact, 183
- Stable isotopes  
High precision measurement of titanium isotope ratios by plasma source mass spectrometry, 21
- Synchrotron radiation  
Photoionisation of ethylene clusters by synchrotron radiation in the energy range 17–50 eV, 281
- Theory  
Expanded theory for the resolving power of a linear ion mobility spectrometer, 399
- Time-of-flight  
Rydberg Matter of K and  $\text{N}_2$ : angular dependence of the time-of-flight for neutral and ionized clusters formed in Coulomb explosions, 127
- Time-of-flight mass spectrometry  
A time-of-flight mass spectrometry study of the fragmentation of valence shell ionised benzene, 31  
A photoionisation mass spectrometry study of the fragmentation of silicon tetrafluoride, tetrachloride and tetrabromide, 359
- TIMS  
Measurement of calcium isotopes ( $\delta^{44}\text{Ca}$ ) using a multicollector TIMS technique, 385
- Titanium isotopes  
High precision measurement of titanium isotope ratios by plasma source mass spectrometry, 21
- Transition metal  
High precision measurement of titanium isotope ratios by plasma source mass spectrometry, 21
- Translational temperature  
Cage effects and rotational hindrance in the surface scattering of large  $(\text{N}_2)_n$  clusters, 159
- Vibrational Feshbach resonances  
High resolution study of cluster anion formation in low-energy electron collisions with molecular clusters of  $\text{CO}_2$ ,  $\text{CS}_2$ , and  $\text{O}_2$ , 313
- Vibrational spectroscopy  
Vibrational spectroscopic evidence of unconventional hydrogen bonds, 289